energies

MDPI

Article

Parameters Identification and Sensitive Characteristics Analysis for Lithium-Ion Batteries of Electric Vehicles

Yun Zhang [1,2], Yunlong Shang [2], Naxin Cui [2] and Chenghui Zhang [2,*]

[1] School of Electrical Engineering, University of Jinan, Jinan 250022, China; xiaoyun9335@163.com
[2] School of Control Science and Engineering, Shandong University, Jinan 250061, China; shangyunlong@mail.sdu.edu.cn (Y.S.); cuinx@sdu.edu.cn (N.C.)
* Correspondence: zchui@sdu.edu.cn; Tel.: +86-531-8839-5717

Received: 15 November 2017; Accepted: 19 December 2017; Published: 22 December 2017

Abstract: This paper mainly investigates the sensitive characteristics of lithium-ion batteries so as to provide scientific basises for simplifying the design of the state estimator that adapt to various environments. Three lithium-ion batteries are chosen as the experimental samples. The samples were tested at various temperatures (−20 °C, −10 °C, 0 °C , 10 °C , 25 °C) and various current rates (0.5C, 1C, 1.5C) using a battery test bench. A physical equivalent circuit model is developed to capture the dynamic characteristics of the batteries. The experimental results show that all battery parameters are time-varying and have different sensitivity to temperature, current rate and state of charge (SOC). The sensitivity of battery to temperature, current rate and SOC increases the difficulty in battery modeling because of the change of parameters. The further simulation experiments show that the model output has a higher sensitivity to the change of ohmic resistance than that of other parameters. Based on the experimental and simulation results obtained here, it is expected that the adaptive parameter state estimator design could be simplified in the near future.

Keywords: sensitive characteristics; lithium-ion batteries; time-varying parameters; electric vehicles

1. Introduction

Nowadays, fossil fuel resources are running out and environmental pollution is serious [1,2]. In response to the energy crisis and the increasing pollution problems, interests in electric vehicles (EVs) have grown in recent years [3]. The battery technology is the key component to achieve these electrical systems [4–6]. Owing to the high-energy density, high-power density, low self-discharge rate and other merits compared with other batteries, lithium-ion batteries have been the first-choice candidate as a power source for EVs [7–10]. However, lithium-ion batteries are less tolerant of abuse. The safety issues of lithium-ion have been an important factor restricting the rapid development of EVs [11]. Accurate estimates for state of charge (SOC), state of health (SOH) and other states are needed over the lifetime of the battery pack in order to lengthen the useful lifetime of batteries. A variety of research has investigated the estimation of SOC and SOH [7,12–18]. However, few studies can obtain good estimate results in various actual conditions. The main reason is that lithium-ion batteries have different performances in different environments in view of its sensitivity to temperature, current rate and other physical-chemical factors. Therefore, precise modeling and accurate state estimation at various actual conditions for such systems have always been big challenges for researchers [19].

We considered time-varying parameters when the state estimator was designed in [7], but the detailed parameter sensitivity analysis was not given. Effective lithium-ion battery models appropriate for electric vehicle thermal management were proposed in [20,21]. However, the models are not suitable for the state estimation applications. In [22], the characteristics of battery packs with parallel-connected lithium-ion battery cells were studied. The information provided by the research results make us have a better understanding of the power battery from different perspectives. However, to the authors' best knowledge, almost no model can be suitable for all kinds of operating ranges of currents and temperatures due to all the parameters being time-varying. Then, the accuracy of battery states is estimated based on the equivalent circuit model will degrade when the operating conditions change. Many studies [14,16,23–28] are based on Kalman filter (KF) and its derivatives to deal with the time-varying parameter and system nonlinear problems. The KF is an optimal recursive estimation method for linear systems under the condition that the noises are Gaussian white noises. Failing to satisfy the conditions, filter divergence will occur [24,28]. The extended KF (EKF) uses a first-order Taylor expansion at each time step to approximate the nonlinear observer function, which will increase the estimation errors due to the local linearization when the battery model has significant nonlinearity (for example, the relationship between open circuit voltage and SOC) [29]. The computation cost of EKF is also tremendous. To be able to accurately estimate the battery states, it is necessary to maintain the nonlinear characterization of the system dynamic [4] and design a new nonlinear adaptive observer instead of EKF for the time-varying parameter system. However, there is no uniform method for nonlinear system observer design. It is a big challenge to design an observer for the battery system because all of the parameters are time-varying. To this end, the sensitive properties of lithium-ion batteries are investigated here by the offline data. Then, we can only consider the parameters whose changes have great influence on the model output when the adaptive nonlinear observer is designed.

Therefore, this paper focuses on the study of the sensitive characteristics for lithium-ion batteries. The main objective of these sensitive characteristics analysis is to find the dominant parameters that influence the battery model accuracy so as to simplify the adaptive parameter state estimator design. A number of experiments and simulations are conducted in order to investigate the sensitive characteristics based on the experimental and simulation results. An accurate electrochemical-polarization model is put forward for the lithium-ion batteries. The model output at 25 °C is used as a reference. Then, the values of model parameters are changed one by one and the model output is recorded at the same time when the same current is applied to the proposed model. Finally, the dominant parameters that influence the model output are found based on the previous data, which provides scientific bases for simplifying the adaptive parameter state estimator.

The remainder of this paper is organized as follows. Section 2 gives the equivalent circuit model for lithium-ion batteries along with its dynamics and model parameters identification method. In Section 3, test bench and experiment procedure are reported. Section 4 presents a sensitive characteristics analysis of battery. This paper ends with some conclusions and suggestions for further studies pertaining to lithium-ion batteries applied in EVs.

2. Battery Modeling and Parameter Identification Method

The principle of selecting a battery model is as simple as possible but precise enough for the investigated problem. The model chosen here is the first-order Thevenin model (see Figure 1), which is simple yet accurate enough for the control-oriented purpose in EVs [30]. The parallel RC-branch, comprising R_p and C_p, is utilized to model the battery polarization effect. R denotes the ohmic resistance and is responsible for the instantaneous voltage drop of the step response. u_{oc} denotes the open circuit voltage and it changes with different capacity levels. u_t denotes the terminal voltage. I denotes the terminal current (current flowing into the battery is considered positive).

Based on Kirchhoff's law, the electrical behavior of the circuit can be characterized as:

$$\begin{cases} \dot{u}_p &= -\frac{1}{C_p R_p} u_p + \frac{1}{C_p} I, \\ u_t &= u_{oc} - RI - u_p, \end{cases} \tag{1}$$

where u_p is the voltage of capacitor C_p. In reality, all parameters of battery systems are multivariable functions of SOC, rate, temperature, etc. Some parameters can maybe be simplified to be independent of some variables, but the others can't be simplified. The study in this paper is unique in that it not only provides the characteristics of battery performance sensitive to the ambient condition, but it also provides the characteristics of battery model output sensitive to the change of parameters.

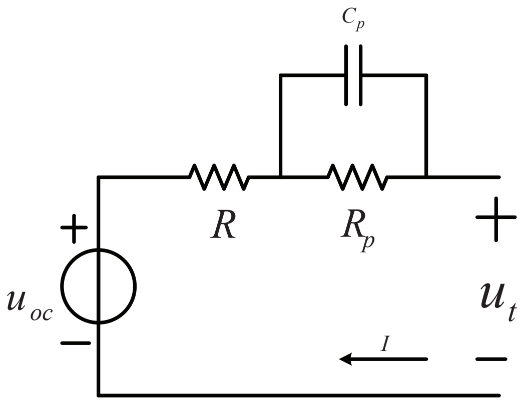

Figure 1. Thevenin equivalent model for lithium-ion batteries.

The parameters R, R_p and C_p can be calculated from the hybrid pulse power characterization (HPPC) test data. The pulsed-discharge experiments are carried out at different SOCs, and the terminal voltage is monitored simultaneously (see Figure 2). The battery parameters can be extracted through the transient response. The terminal voltage response at different SOCs can be fitted as in the following form:

$$u_t(t) = V_2 + c_1(1 - e^{-c_2 t}), \tag{2}$$

where c_1 and c_2 are the least-squares curve fitting coefficients. Then, the parameters value of battery model (see Figure 1) can be derived from:

$$R = \frac{V_2 - V_1}{I}, \ R_p = \frac{c_1}{I}, \ C_p = \frac{1}{c_2 R_p}. \tag{3}$$

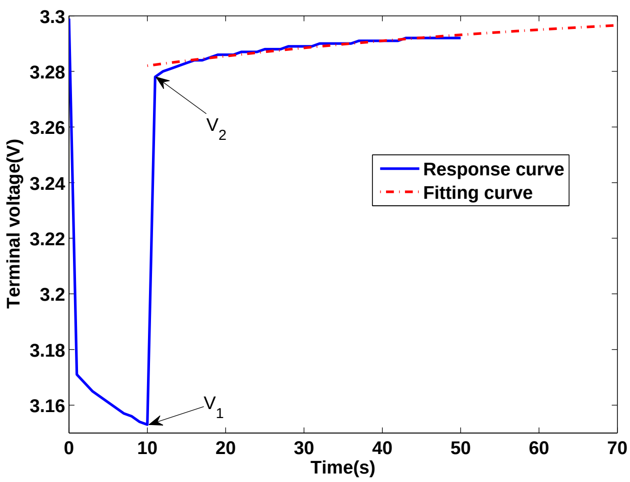

Figure 2. Terminal voltage response under step–current discharge.

3. Experiment

3.1. Test Bench

The Meikai Lin (MKL) battery tester shown in Figure 3a is designed to charge and discharge the batteries (see Figure 3b). The batteries are placed in the temperature chamber for environment control. Current and voltage data are collected from the high precision current and voltage transducers through I-Solution, a built-in software of MKL.

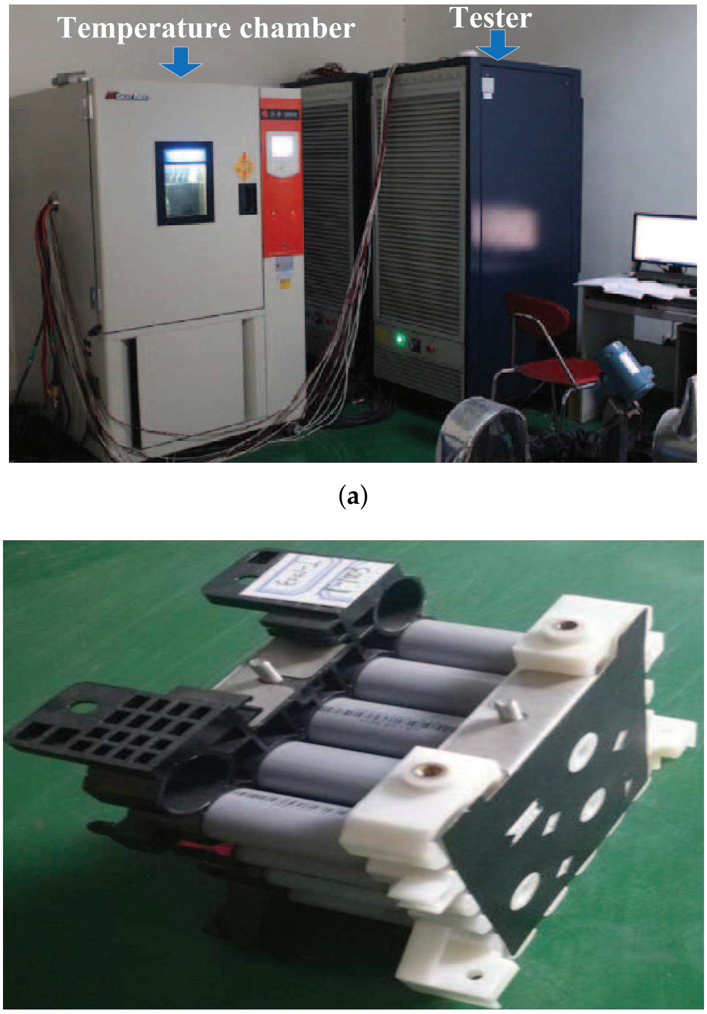

(**a**)

(**b**)

Figure 3. Test bench: (**a**) MKL battery tester and (**b**) 32 Ah battery.

3.2. Test Samples and Experiment Procedure

Three $LiFePO_4$ 18650 batteries (twenty cells wired in parallel) with 32 Ah rated capacity and 3.2 V nominal voltage are used for all cycling tests. The charging strategy is the constant-current and constant-voltage strategy. The constant current is $\frac{1}{3}$C (namely $\frac{1}{3} \times 32 \approx 10.67$ A) and the constant-voltage is 3.65 V. The charging current cutoff point is set to be 0.02C for the constant-voltage charging stage. The discharge procedure is as follows: the batteries are fully charged firstly, they are left in the open-circuit condition for a long enough period and then the hybrid pulse power characterization (HPPC) experiment is carried out. The discharge current I_d is 1C and the charge current I_c is 0.75C. Afterwards, they are discharged at a constant current of 0.5C (see Figure 4a) from the fully charged state to 95% of the nominal capacity. The foregoing procedure is repeatedly performed until the batteries are fully discharged. The cutoff voltage point of the cell module is set to be 2 V. The same experimental procedure were carried out with a current of Figure 4c,e at different temperatures (−20 °C , −10 °C, 0 °C, 10 °C, 25 °C). When applying the current to the battery, the terminal voltage is monitored simultaneously (see Figure 5a,c,e).

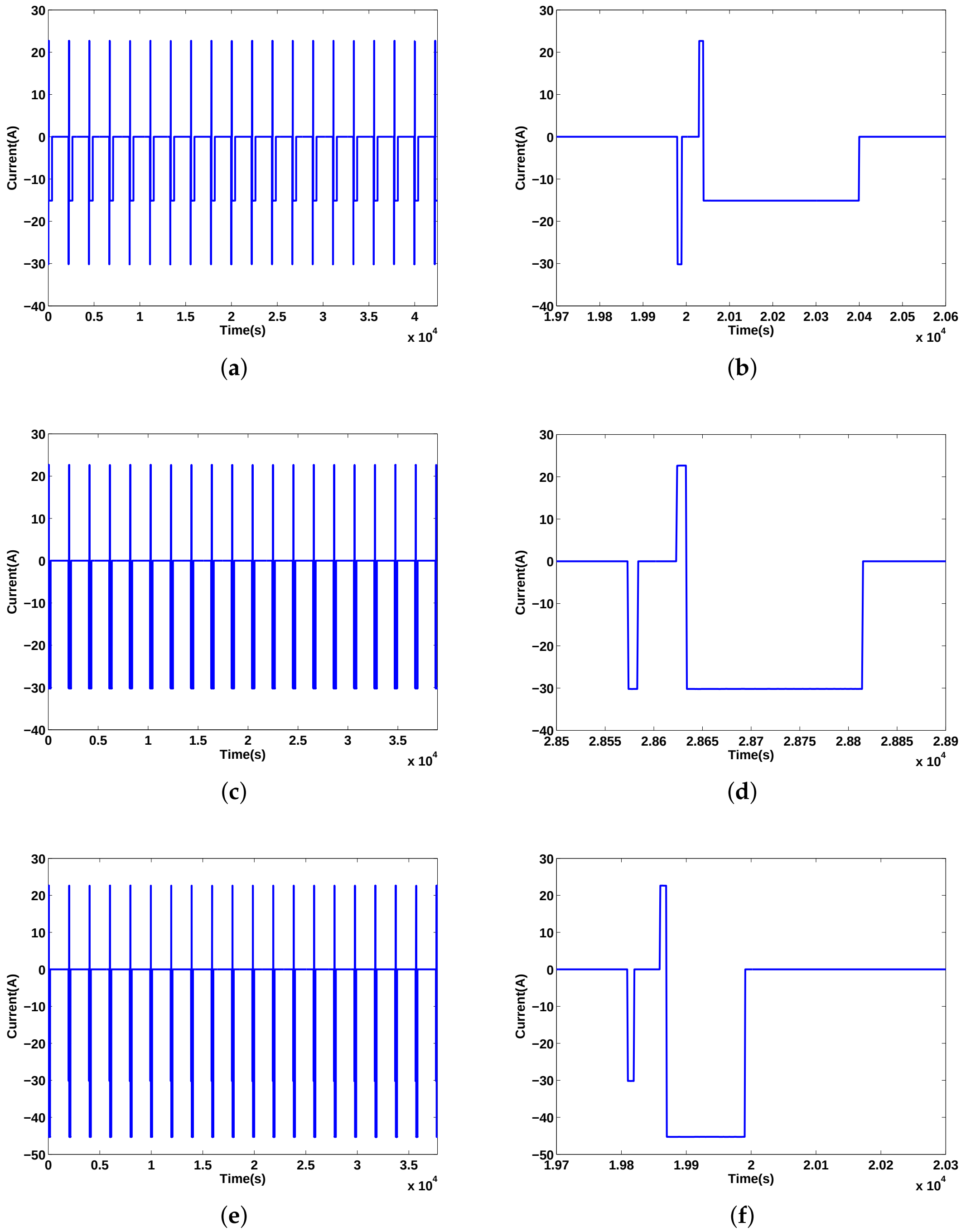

Figure 4. Testing cycle currents: (**a**) pulse and 0.5C constant current; (**c**) pulse and 1C constant current and (**e**) pulse and 1.5C constant current; (**b**), (**d**) and (**f**) are the zoom of (**a**), (**c**) and (**e**), respectively.

4. Sensitivity Characteristics Analysis

4.1. Battery Sensitivity Analysis

4.1.1. The Sensitivity of Battery Output Voltages to Temperature and Current Rate

Figure 5a,c,e are the battery output voltage curves obtained when the currents of Figure 4a,c,e were applied to the batteries. It can be seen that no more than 50% of the battery energy is available at −20 °C. Generally speaking, higher internal resistance at low temperature, creating a high opposing fore while operating the battery, and which will limit the amount of energy extracted and reduce cell energy and power capability [4,5]. The output voltages of batteries will drop with the temperature drop, and this phenomenon will be more obvious with the current rate increasing. The voltage rate of change (ROC) is used to measure the percentage change in battery output voltage and calculated by $(battery^{25} - battery^{10})/battery^{25} \times 100\%$ are depicted in Figure 5b,d,f ($battery^{10}$ and $battery^{25}$ represent battery output voltage at 10 °C and 25 °C, respectively). The ROCs are approximately within 2% (see Figure 5b), 3% (see Figure 5d), and 6% (see Figure 5f) throughout the whole SOC. The battery output voltage ROC will increase as the temperature ROC becomes larger and the other ROC curves of battery output voltage are omitted for brevity. The experimental results show that battery output voltages will be different with the same current applied to them at different temperature. Under the same temperature ROC conditions, the larger the "same current" becomes, the larger the battery output difference will be.

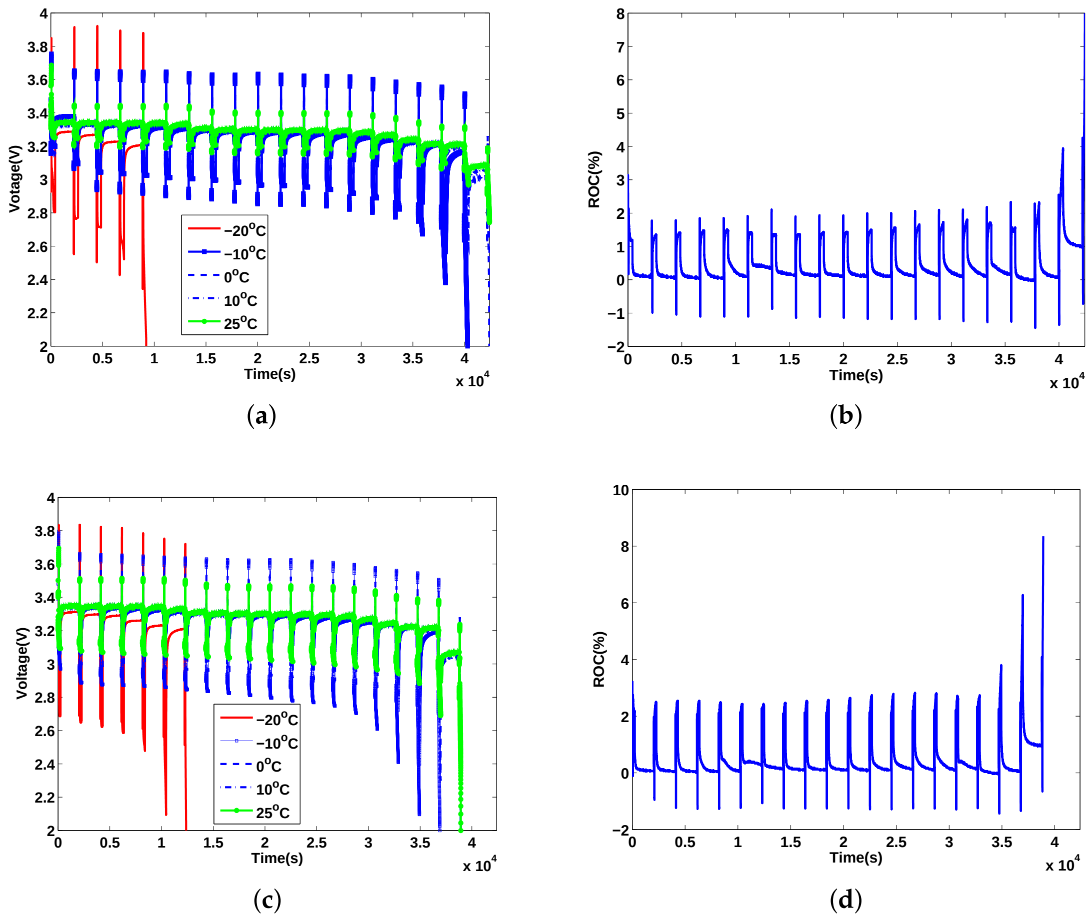

Figure 5. *Cont.*

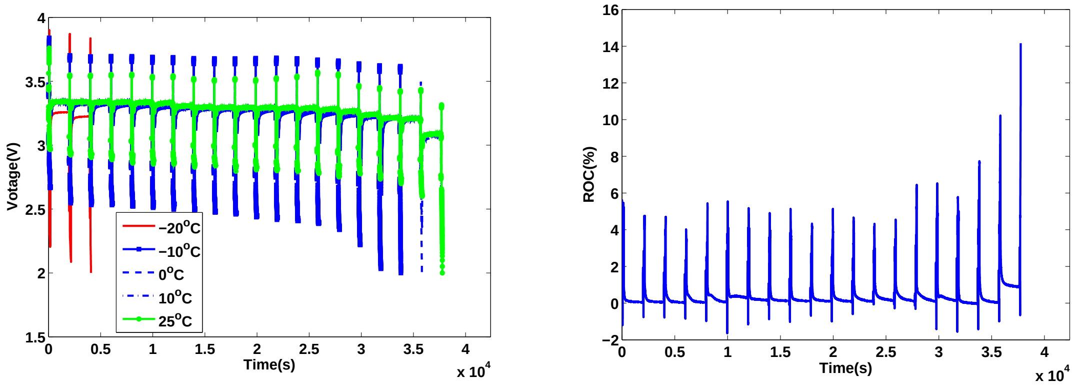

(**e**) (**f**)

Figure 5. Experimental pulse discharge curves at various temperatures with a discharge current of: (**a**) Figure 4a; (**c**) Figure 4c and (**e**) Figure 4e and the ROC curves (**b**); (**d**) and (**f**).

4.1.2. The Sensitivity of Battery Parameters to SOC, Temperature and Current Rate

The parameter values identified for battery model at different SOCs, different temperatures and different current rates are depicted in Figure 6a–i. From Figure 6a,d,g, it can be seen that ohmic resistance R is sensitive to temperature and current rate. Small parameter differences among the curves for different SOCs indicate that parameter R is approximately independent of SOC, especially within the range of 10–90% SOC. The curves of Figure 6b,e,h show that R_p are sensitive to temperature and SOC but less sensitive to current rate. The parameter C_p is sensitive to temperature but less sensitive to current rate and SOC can be seen from the curves of Figure 6c,f,i. From the above analysis, we can see that all of the extracted RC parameters are sensitive to temperature, and partial parameters are sensitive to SOC and current rate. From −10 °C to 25 °C, a range within the main operating temperature range of −10 °C to 50 °C of lithium-ion batteries [31], R reduces approximately three times, R_p reduces approximately six times and C_p increases approximately six times throughout the whole SOC range. Since the parameters change so much during battery operation, it is necessary to thoroughly analyze the effect of parameter changes on the accuracy of battery model. Especially in the applications of EVs, the parameters change will be larger than other applications because the current rate and temperature change are relatively large [32]. However, some research results do not consider the change of parameters [21,33] when modeling, and which will further lead to the accuracy decline of model-based state estimation .

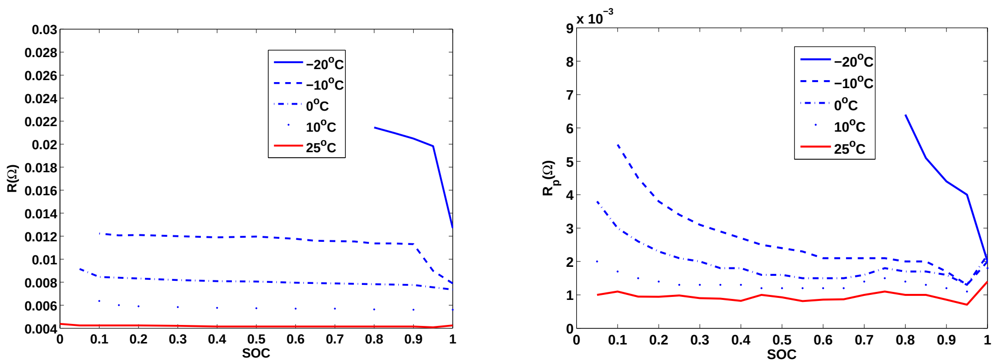

(**a**) (**b**)

Figure 6. *Cont.*

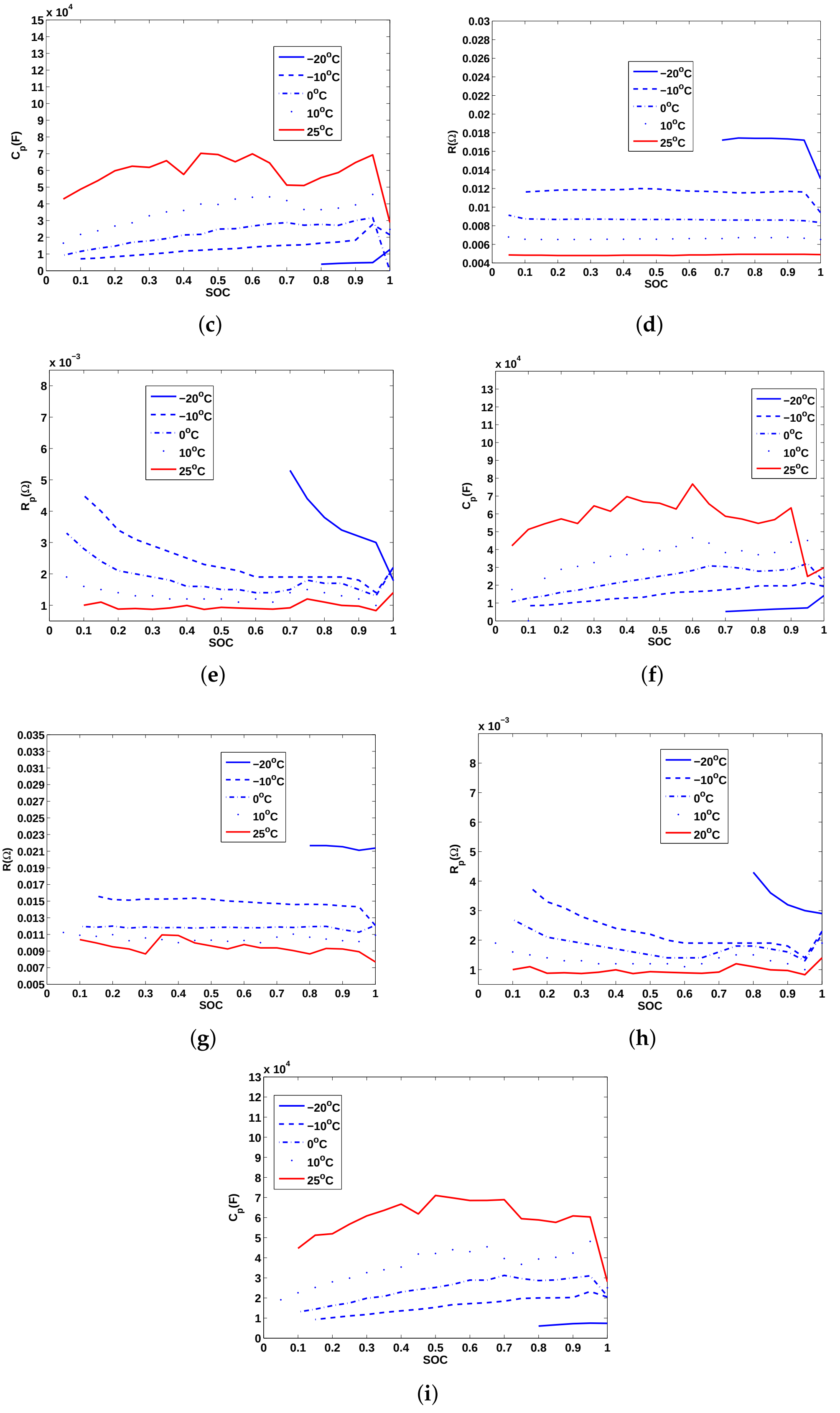

Figure 6. Experimental results for R-SOC, R_p-SOC, C_p-SOC at various temperatures. (**a**–**c**) applied the current of Figure 4a to the battery; (**d**–**f**) applied the current of Figure 4c to the battery; (**g**–**i**) applied the current of Figure 4e to the battery.

4.1.3. The Sensitivity of the Relationship u_{oc}-SOC to Temperature and Current Rate

Open-circuit voltage (u_{oc}) is one of the most important parameters of a battery due to the relationship between SOC and open-circuit voltage (u_{oc}) [12,23,34–39], which is defined as the measured terminal voltage when battery reaches steady-state. Figure 7a–c show the relationships between open circuit voltage (u_{oc}) and SOC at different temperatures and different current rates. Figure 7a–c show that the curves at various temperatures are basically consistent except for the curve at the extreme temperature −20 °C. The average value curves at −10 °C, 0 °C, 10 °C and 25 °C with the discharge rates 0.5C, 1C and 1.5C are depicted in Figure 7d. It can be seen that the three average value curves are also basically consistent. The curve fitting for the three average value curves is depicted in Figure 7e. Therefore, it can be obtained that the relationship between open circuit voltage (u_{oc}) and SOC has a better consistency and low sensitivity to temperature and rate except for the extreme low temperature condition −20 °C (the diffusivity of Li^+ ions inside the cell will decrease at an extreme low temperature [40]). Then, the single-variable function used to represent the fitting curve (the blue line dotted by ∇ in Figure 7e) can be obtained by utilizing the nonlinear least-squares fitting method:

$$u_{oc} = 3.2341 + 0.1173\mathrm{SOC} + 0.003\mathrm{SOC}^2 - 0.5376e^{-20.4447\mathrm{SOC}}. \quad (4)$$

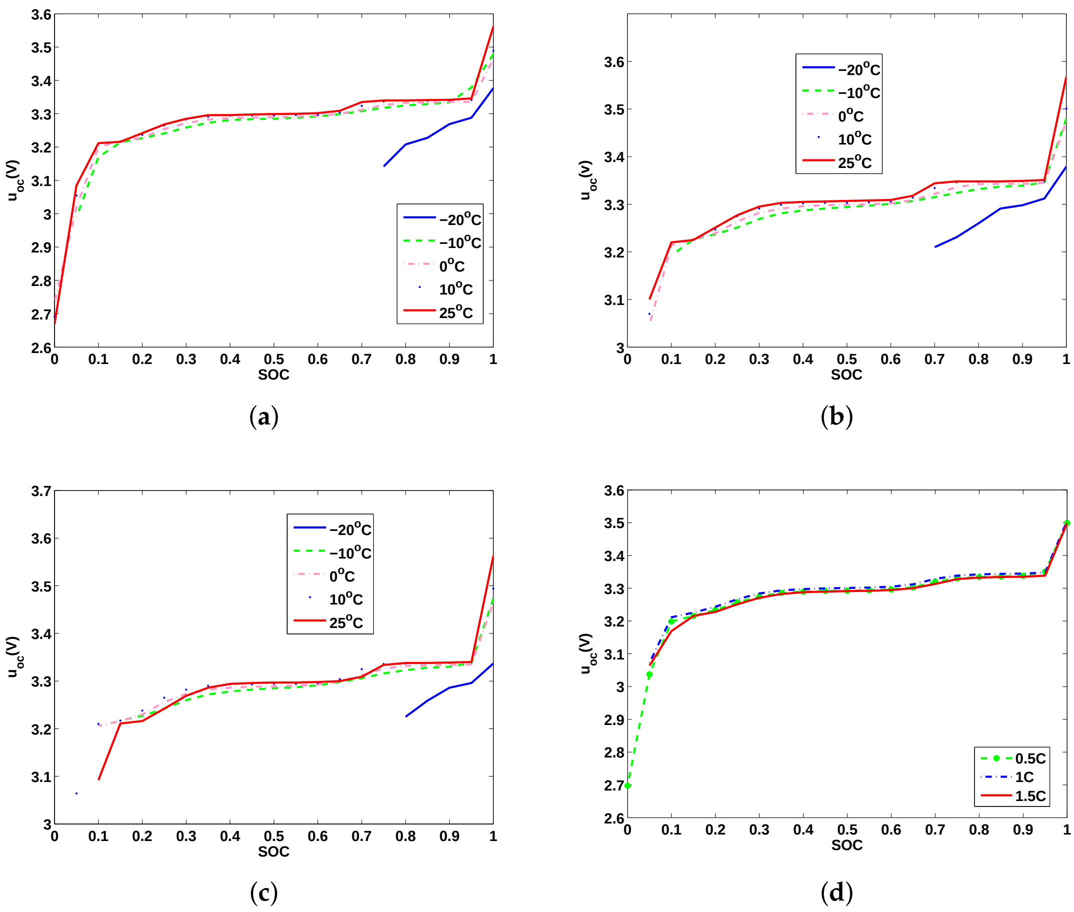

(**a**) (**b**) (**c**) (**d**)

Figure 7. *Cont.*

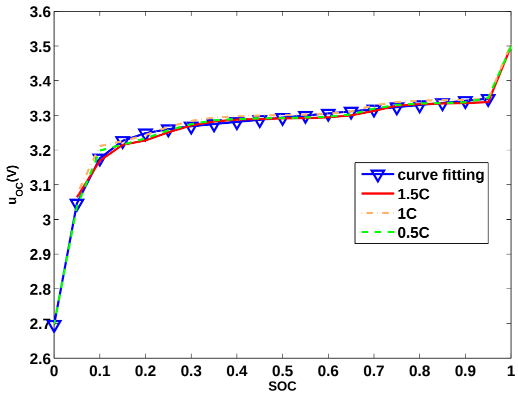

(**e**)

Figure 7. U_{oc} against SOC for the lithium-ion batteries. (**a**) discharging current of Figure 4a; (**b**) discharging current of Figure 4c; (**c**) discharging current of Figure 4e; (**d**) the average value curves for u_{oc}-SOC at temperature −10 °C, 0 °C, 10 °C and 25 °C; (**e**) the fitting curve for the three average value curves of (**d**).

4.2. The Sensitivity of Battery Model Output to Change of Parameters

4.2.1. Model Validation

To validate the extracted model of the lithium-ion battery, we choose battery output voltage at 25 °C with the discharge of Figure 4a as a reference and compare the battery output with the model output. The parameters that were extracted from the corresponding experimental data were applied to the model. The simulation results against experimental data is shown in Figure 8a. SOC defined in Equation (5) changes from 1 to 0 throughout the whole procedure (see Figure 4b):

$$SOC = SOC_{ini} - \frac{\int_0^t I(t)dt}{C_N}. \tag{5}$$

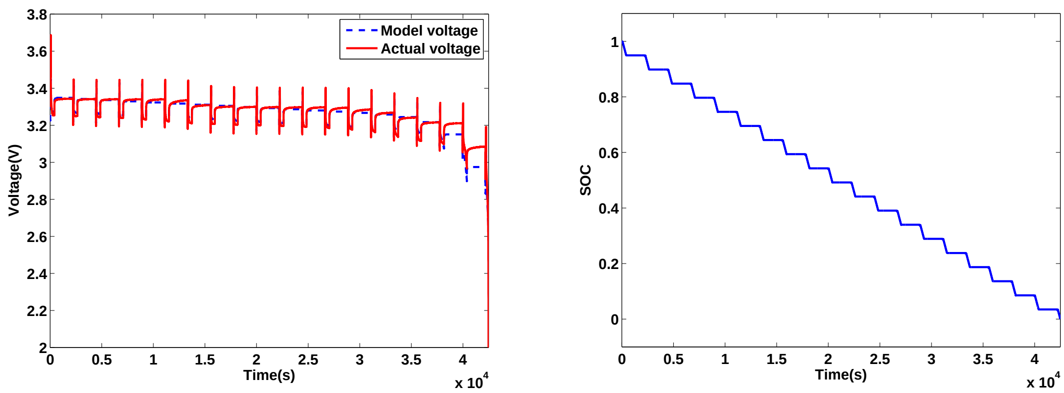

(**a**) (**b**)

Figure 8. Comparison between voltage response of the battery and the battery model throughout the whole range of SOC with the discharge current of Figure 4a. (**a**) Measured and modeled battery voltage; (**b**) SOC with experiment.

The maximum modeling error is 1.23% and the average error is 0.29% within the range over 15–95% SOC (lithium-ion battery mostly operated over 20–80% SOC to protect the battery from irreversible damage). How does model output change when operating conditions change? In other words, how do the changes of battery parameters affect the model output? The detailed analysis based on this model will be given in the next section.

4.2.2. The Effect of Parameters Change on Model Output Analysis

In Figure 9, the voltages ut^{25}, ut^{10} and ut^{-10} denote the model outputs when the parameters extracted from the experimental data at 25 °C, 10 °C or −10 °C are applied to the proposed model, respectively. Voltages ut^{Cp10}, ut^{Rp10}, ut^{R10}, ut^{Cp-10}, ut^{Rp-10} and ut^{R-10} denote model outputs when the value of the parameter C_p, R_p or R extracted from the experimental data at 25 °C are replaced with the value extracted from the experimental data at 10 °C or −10 °C, respectively. The model output voltage ut^{25} is selected as a reference and the model output voltage ROC (for example $ROC_{ut^{25}}^{ut^{10}}$ defined in (6)) is depicted in Figure 9a,c,e:

$$ROC_{ut^{25}}^{ut^{10}}(\%) = \frac{ut^{10} - ut^{25}}{ut^{25}} * 100\%. \tag{6}$$

From the simulation results, it can be seen that the change of ohmic resistance R has the greatest influence on the model output regardless of constant current (Figure 9a) or alternate current (Figure 9c,e) applied to batteries. The changes of C_p and R_p have little effect on the model output. From −10 °C to 25 °C, although $ROC_{ut^{25}}^{ut^{-10}}$ reaches 10%, $ROC_{ut^{25}}^{ut^{Cp-10}}$ only is 0.1% and $ROC_{ut^{25}}^{ut^{Rp-10}}$ is no more than 0.6%. The change of model output is mainly affected by the change of parameter R.

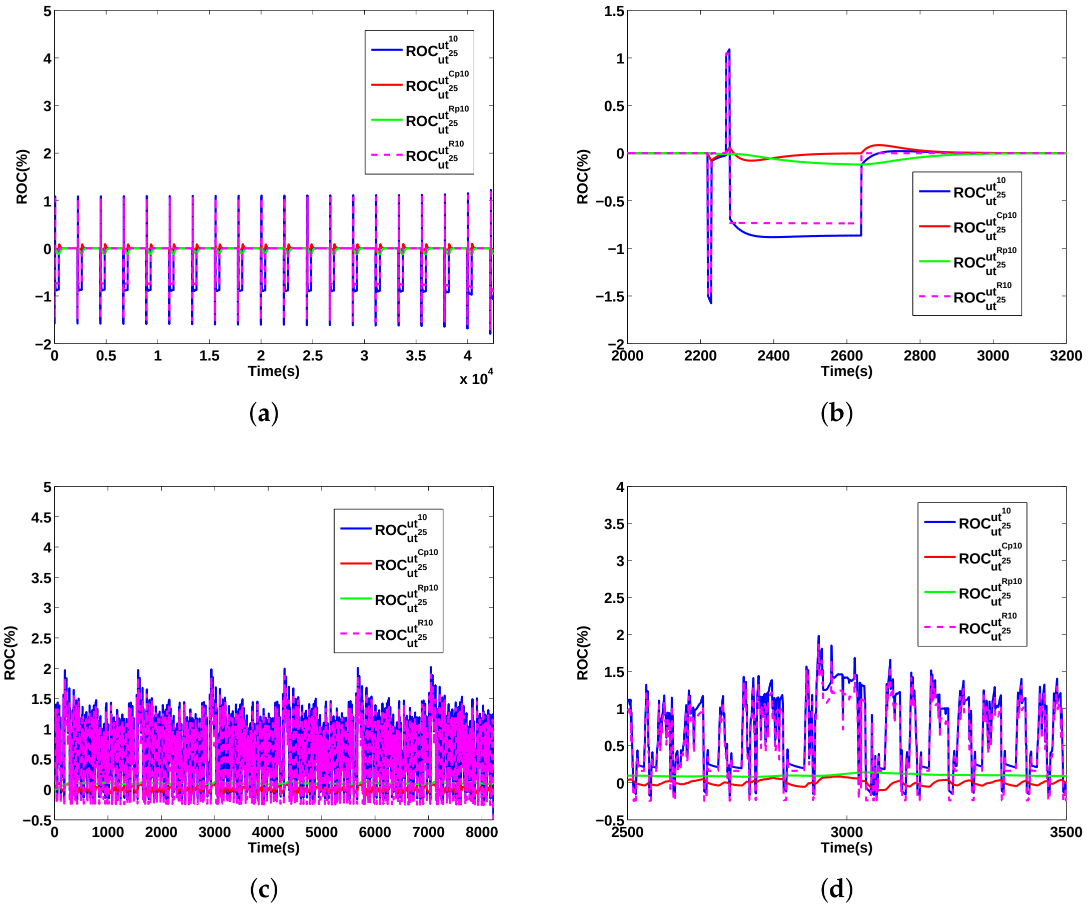

Figure 9. *Cont.*

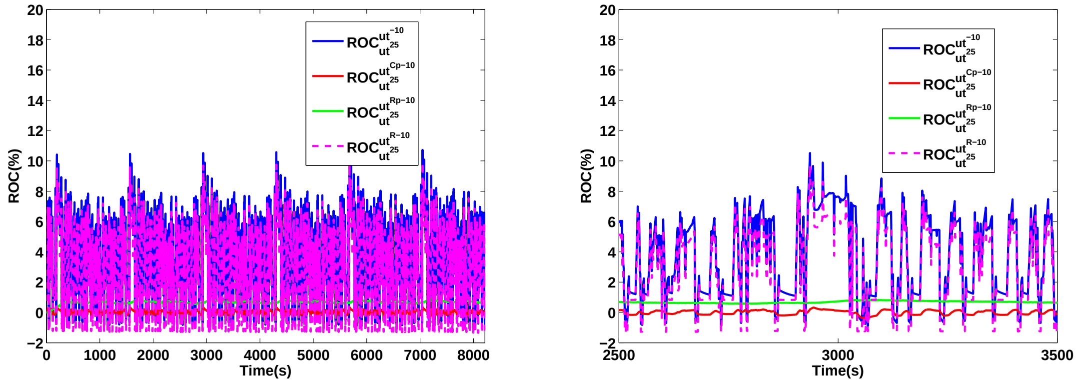

(**e**) (**f**)

Figure 9. The model output voltage rate of change when the model parameters change: (**a**) with the current of Figure 4a; (**c**) and (**e**) with the alternative current; (**b**); (**d**) and (**f**) are the zoom of (**a**); (**c**) and (**e**), respectively.

4.3. Discussion

The output characteristics of lithium-ion batteries are sensitive to temperature and current rate because of physical and chemical reactions coexisting in batteries. An accurate, intuitive and comprehensive electrical model, which includes R, R_p, C_p and u_{oc}, has been selected to capture the dynamic characteristics of a battery. The modeling accuracy will degrade when operate conditions change due to the fact that model parameters are time-varying. Parameters R, R_p and C_p will have several times change from −10 °C to 25 °C throughout the whole SOC. However, only the change of parameter R has an obvious effect on the model output. Then, we can simplify the design procedure of model-based adaptive parameter state estimators. The parameters and SOC are both estimated in [27,28]. In [27], the SOC is estimated based on an EKF and the obtained results are satisfactory under various laboratory conditions. However, obtaining good estimates of the results not only need voltage and current signals, but also the temperature signal. The computational complexity of the robust and accurate estimation strategies proposed in [28] is high. In order to ensure the accuracy of estimation under actual operating conditions, it is necessary to design a nonlinear observer that does not need such model local linearization as EKF needs. The nonlinear observer to be designed only needs voltage and current signals.

In much literature, (see [2,13–16,27]), the ohmic resistance R or the sum of the ohmic resistance R and the polarization resistance R_p is used as an indicator for the SOH of batteries, but they are not the best choice of estimating the SOH on board due to the sensitivity of parameters to battery states, temperature and other factors [41]. To find more effective assessment indicators of SOH is also an important research direction.

5. Conclusions

This paper has mainly investigated the sensitivity of the lithium-ion battery to temperature and current rate. Through various experimental tests and simulations, the sensitive characteristics of batteries have been analyzed and discussed. The experimental and simulation results reveal the following findings: (1) from −10 °C to 25 °C, the ohmic resistance R decreases approximately three times, the polarization resistance R_p decreases approximately six times and the polarization C_p increases approximately six times; (2) from −10 °C to 25 °C, the relationship of u_{oc}-SOC is basically stable; (3) the ROC of model output reaches 10% when applied the parameters values obtained from the experiment data at −10 °C and 25 °C to the model, respectively, but ROCs of model output caused by the changes of parameters R_p and C_p only are 0.6% and 0.1%; and (4) developing the adaptive nonlinear observer design theory and method specifically for battery systems with strong time-varying and nonlinear characteristics can promote the development of battery management technology more effectively. The conclusions obtained here offer battery management system researchers the possibility to understand the sensitive characteristics of the lithium-ion batteries more profoundly. Our next work is to find more effective assessment indicators of SOH and design a nonlinear adaptive observer for battery state estimates.

Acknowledgments: This work is supported by the National Natural Science Foundation of China under Grants 61403162, the Major Scientific Instrument Development Program of the National Natural Science Foundation of China under Grant No. 61527809, the Key Project of National Natural Science Foundation of China under Grant No. 61633015, and the National Natural Science Foundation of China under Grants 61403061.

Author Contributions: Yun Zhang conceived this paper, designed and performed the experiments, and analyzed the data; Yunlong Shang and naxin Cui revised the paper; and Chenghui Zhang revised the paper and provided some valuable suggestions.

Conflicts of Interest: The authors declare no conflict of interest.

Nomenclature: $battery^{10}$, battery output voltage at 10 °C; $battery^{25}$, battery output voltage at 25 °C; C, capacity [Ah]; c_1, c_2, fitted parameter; I, current [A]; R, resistance [Ω]; R_p, resistance [Ω]; t, time[s]; u_{oc}, open circuit voltage; u_t, terminal voltage; ut^{-10}, ut^{10}, ut^{25}, model output voltage when the parameters extracted from the experimental data at −10 °C, 10 °C, or 25 °C are applied to the proposed model; ut^{Cp-10}, ut^{Rp-10} , ut^{R-10}, ut^{Cp10}, ut^{Rp10}, ut^{R10}, model output voltage when the value of the parameter C_p, R_p or R extracted from the experimental data at 25 °C is replaced with the value extracted from the experimental data at −10 °C or 10 °C; V, voltage [V]
Subscripts: c, charge; d, discharge; ini, initial; N, nominal; oc, open circuit; p, polarization; t, terminal
Acronyms: A, Ampere; EVs, Electric Vehicles; EKF, Extended Kalman Filter; HPPC, Hybrid Pulse Power Characterization; KF, Kalman Filter; $LiFePO_4$ 18650, $LiFePO_4$ means Lithium Iron Phosphate, 18650 means 18-mm diameter, and 650 means 65-mm height; MKL, Meikai Lin; ROC, Rate of change; SOC, State of charge; SOH, State of health

References

1. Landi, M.; Gross, G. Measurement techniques for online battery state of health estimation in vehicle-to-grid applications. *IEEE Trans. Instrum. Meas.* **2014**, *63*, 1224–1234.
2. Tsang, K.M.; Chan, W.L. State of health detection for lithium ion batteries in photovoltaic system. *Energy Convers. Manag.* **2013**, *65*, 7–12.
3. Xioing, R.; Cao, J.Y.; Yu, Q.Q. Reinforcement learning-based real-time power management for hybrid energy storage system in the plug-in hybrid electric vehicle. *Appl. Energy* **2018**, *211*, 538–548.
4. Panchal, S.; Mcgrory, J.; Kong, J.; Fraser, R.; Fowler, M.; Dincer, I.; Agelin-Chaab, M. Cycling degradation testing and analysis of a $LiFePO_4$ battery at actual conditions. *Int. J. Energy Res.* **2017**, *41*, 2565–2575.
5. Jaguemont, J.; Boulon, L.; Dubé, Y. A comprehensive review of lithium-ion batteries used in hybrid and electric vehicles at cold temperatures. *Appl. Energy* **2016**, *164*, 99–114.
6. Xiong, R.; Cao, J.Y.; Yu, Q.Q.; He, H.W.; Sun, F.C. Critical review on the battery state of charge estimation methods for electric vehicles. *IEEE Access* **2017**, doi:10.1109/ACCESS.2017.2780258.
7. Zhang, Y.; Zhang, C.H.; Zhang, X.F. State-of-charge estimation of the lithium-ion battery system with time-varying parameter for hybrid electric vehicles. *IET Control Theory Appl.* **2014**, *8*, 160–167.
8. Shang, Y.L.; Zhang, C.H.; Cui, N.X.; Guerrero, J.M. A cell-to-cell battery equalizer with zero-current swithcing and zero-voltage gap based on quasi-resonant LC converter and boost converter. *IEEE Trans. Power Electron.* **2015**, *30*, 3731–3747.
9. Haidar, A.M.A.; Muttaqi, K.M. Behavioral characterization of electric vehicle charging loads in a distribution power grid through modeling of battery chargers. *IEEE Trans. Ind. Appl.* **2016**, *52*, 483–492.
10. Chaoui, H.; Gualous, H. Online parameter and state estimation of lithium-ion batteries under temperature effects. *Electr. Power Syst. Res.* **2017**, *145*, 73–82.
11. Panchal, S.; Dincer, I.; Agelin-Chaab, M.; Fraser, R.; Fowler, M. Design and simulation of a lithium-ion battery at large C-rates and Varying boundary conditions through heat flux distributions. *Measurement* **2018**, *116*, 382–390, doi:10.1016/j.measurement.2017.11.038.
12. Lee, S.; Kim, J.; Lee, J.; Cho, B.H. State-of-charge and capacity estimation of lithium-ion battery using a new open-circuit voltage versus state-of-charge. *J. Power Sources* **2008**, *185*, 1367–1373.

13. Gould, C.R.; Bingham, C.M.; Stone, D.A.; Bentley, P. New battery model and state-of-health determination through subspace parameter estimation and state-observer techniques. *IEEE Trans. Veh. Technol.* **2009**, *58*, 3905–3919.
14. Kim, J.; Cho, B.H. State-of-charge estimation and state-of-health prediction of a Li-ion degraded battery based on an EKF conmbined with a per-unit system. *IEEE Trans. Veh. Technol.* **2011**, *60*, 4249–4260.
15. Remmlinger, J.; Buchholz, M.; Meiler, M.; Bernreuter, P.; Dietmayer, K. State-of-health monitoring of lithium-ion batteries in electric vehicles by on-board internal resistance estimation. *J. Power Sources* **2011**, *196*, 5357–5363.
16. Andre, D.; Nuhic, A.; Soczka-Guth, T.; Sauer, D.U. Comparative study of a structured neural network and an extended Kalman filter for state of health determination of lithium-ion batteries in hybrid electric vehicles. *Eng. Appl. Artif. Intell.* **2013**, *26*, 951–961.
17. Dang, X.J.; Yan, L.; Jiang, H.; Wu, X.R.; Sun, H.X. Open-circuit voltage-based state of charge estimation of lithium-ion power battery by combining controlled auto-regressive and moving average modeling with feedforward-feedback compensation method. *Electr. Power Energy Syst.* **2017**, *90*, 27–36.
18. Li, M.H. Li-ion dynamics and state of charge estimation. *Renew. Energy* **2017**, *100*, 44–52.
19. Hussein, A.A. Capacity fade estimation in electric vehicle li-ion batteries using artificial neural networks. *IEEE Trans. Ind. Appl.* **2015**, *51*, 2321–2330.
20. Jaguemont, J.; Boulon, L.; Dubé, Y. Characterization and modeling of a hybrid-electric-vehicle lithium-ion battery pack at low temperatures. *IEEE Trans. Veh. Technol.* **2016**, *65*, 1–14.
21. Tan, Y.K.; Mao, J.C.; Tseng, K.J. Modeling of battery temperature effect on electrical characteristics of Li-ion battery in hybrid electric vehicle. In Proceedings of the 9th IEEE International Conference on Power Electronics and Drive Systems, Singapore, 5–8 December 2011; pp. 637–642.
22. Gong, X.Z.; Xiong, R.; Mi, C.C. Study of the characteristics of battery packs in electric vehicles with parallel-connected lithium-ion battery cells. *IEEE Trans. Ind. Appl.* **2015**, *51*, 1872–1879.
23. Vasebi, A.; Partovibakhsh, M.; Taghi, S. A novel combined battery model for state of charge estimation in lead acid batteries based on extended Kalman filter for hybrid electric vehicle application. *J. Power Sources* **2007**, *174*, 30–40.
24. He, H.; Xiong, R.; Zhang, X.; Sun, F.; Fan, J. State-of-charge estimation of the lithium-ion battery using an adaptive extended kalman filter based on an improved thevenin model. *IEEE Trans. Veh. Technol.* **2011**, *60*, 1461–1469.
25. Yuan, S.; Wu, H.; Yin, C. State of charge estimation using the extended kalman filter for battery management systems based on the arx battery model. *Energies* **2013**, *6*, 444–470.
26. Xing, Y.J.; He, W.; Pecht, M.; Tsui, K.L. State of charge estimation of lithium-ion batteries using the open-circuit voltage at various ambient temperatures. *Appl. Energy* **2014**, *113*, 106–115.
27. Mejdoubi, A.E.; Oukaour, A.; Chaoui, H.; Gualous, H.; Sabor, J.; Siamani, Y. State-of-charge and state-of-health lithium-ion batteries' diagnosis according to surface temperature variation. *IEEE Trans. Ind. Electron.* **2016**, *63*, 2391–2402.
28. Yu, Q.Q.; Xiong, R.; Lin, C.; Shen, W.X.; Deng, J.J. Lithium-ion battery parameters and state-of-charge joint estimation based on H-infinity and unscented Kalman filters. *IEEE Trans. Veh. Technol.* **2017**, *66*, 8693–8701.
29. Xia, B.; Zheng, W.H.; Zhang, R.F.; Lao, Z.Z.; Sun, Z. A novel observer for lithium-ion battery state of charge estimation in electric vehicles based on a second-order equivalent circuit model. *Energies* **2017**, *10*, 1150, doi:10.3390/en10081150.
30. Tian, S.; Hong, M.N.; Ouyang, M.G. An experimental study and nonlinear modeling of discharge I-V behavior of valve-regulated lead-acid batteries. *IEEE Trans. Energy Convers.* **2009**, *24*, 452–458.
31. Malik, M.; Dincer, I.; Rosen, M. Review on use of phase change materials in battery themal management for electric and hybrid electric vehicles. *Int. J. Energy Res.* **2016**, *40*, 1011–1031.
32. Van Bree, P.J.; Veltman, A.; Hendrix, W.H.A.; van den Bosch, P.P.J. Prediction of battery behavior subject to high-rate partial state of charge. *IEEE Trans. Veh. Technol.* **2009**, *58*, 588–595.
33. Bhide, S.; Shim, T. Novel predictive electric Li-ion battery model incorporating thermal and rate factor effects. *IEEE Trans. Veh. Technol.* **2011**, *60*, 819–829.
34. Bhangu, B.S.; Bentley, P.; Stone, D.A.; Bingham, C.M. Nonlinear observers for predicting state-of-charge and state-of-health of Lead-acid Batteries for hybrid-electric vehicles. *IEEE Trans. Veh. Technol.* **2005**, *54*, 783–794.

35. Han, J.; Kim, D.; Sunwoo, M. State-of-charge estimation of lead-acid batteries using an adaptive extended Kalman filter. *J. Power Sources* **2009**, *188*, 606–612.
36. Windarko, N.A.; Choi, J. SOC estimation based on OCV for NiMH batteries using an improved Takacs model. *J. Power Electron.* **2010**, *10*, 181–186.
37. Shahriari, M.; Arrokhi, M. FOnline state-of-health estimation of VRLA batteries using state of charge. *IEEE Trans. Ind. Electron.* **2013**, *60*, 191–202.
38. Gholizadeh, M.; Salmasi, F. Estimation of state of charge, unknown nonlinearities, and state of health of a lithium-ion battery based on a comprehensive unobservable model. *IEEE Trans. Ind. Electron.* **2014**, *61*, 1335–1344.
39. Xiong, R.; Zhang, Y.Z.; He, H.W.; Zhou, X.; Pecht, M.G. A double-scale, particle-filtering, energy state prediction algorithm for lithium-ion batteries. *IEEE Trans. Ind. Electron.* **2018**, *65*, 1526–1538.
40. Wang, J.; Liu, P.; Hicks-Garner, J.; Sherman, E.; Soukiazian, S.; Verbrugge, M.; Tataria, H.; Musser, J.; Finamore, P. Cycle-life model for graphite-$LiFePO_4$ cells. *J. Power Sources* **2011**, *196*, 3942–3948.
41. Xiong, R.; Tian, J.P.; Mu, H.; Wang, C. A systematic model-based degradation behavior recognition and health monitoring method for lithium-ion batteries. *Appl. Energy* **2017**, *207*, 372–383.